Hybrid Power System for a Cochlear Implant

Brian Frost
Electrical Engineering PhD Candidate
Columbia University
Email: bf2458@columbia.edu

***Abstract*—Low power medical implant developments have opened up the possibility for fully implantable medical implants in the near future. A less explored route paved by this new technology, however, is the application of low power implants with conventional implant sytems in which the user wears a battery-powered transmitter external to their body. Using low-power circuitry on the implanted receiver side allows for lower power transmitters, which also makes hybrid power supplies significantly more viable. Fully implantable cochlear implant research has promised single miliwatt operation. While this technology remains in development due to other complications to do with fully implantable devices, we propose a scheme herein which leverages this technology to create a traditional cochlear implant with lower power transmission, using a hybrid power system. More specifically, we look to combine solar power with traditional hearing aid batteries to greatly improve battery life. We also present a prototype built on a solderless breadboard, as well as a sample printed circuit board design as validation that this device could meet the size requirements of a cochlear implant transmitter. We find that in direct sunlight the device can be run entirely off of solar power reasonably, and that somewhat frequent exposure to sunlight will allow the device to operate for far longer than it usually would on a single charge.**

I. Introduction

Cochlear implants operate electrically rather than mechanically, stimulating the sensory structures of the inner ear through an implanted electrode array. The implant acts as a receiver, which obtains both an audio signal and power from an external transmitter worn by the user. The external device is worn above the ear, and consists of a microphone, digital signal processor (DSP) and signal/power transmitter. These devices are often rechargeable, although some use one-time-use batteries. Battery life depends on the manufacturer, but usually is in the range of one to two days.

We look to design and construct a model of a transmitter with superior battery life to those employed on the market today. To achieve this, a hybrid power system using both a rechargeable battery and a solar cell is used. We have built a prototype of such a system wherein the DSP units at the transmitter (TX) and receiver (RX), as well as the electrode, are modeled as fixed power-consuming loads – that is to say that this prototype does not contain any signaling circuitry, but only the circuitry related to power transmission. We have constructed both the hybrid power source and the radio frequency (RF) link for power transmission, and we model the channel (simply a fixed distance between RX and TX) to achieve an estimated power consumed by the device.

II. Literature Review

A. The RF Link

Wireless power transfer is most often implemented through resonant coupled coils. The company Infineon has written a short document explaining the principle behind wireless charging, in which they describe the coupling between the TX and RX circuits. The circuit in Figure 1 is the circuit at the heart of wireless power transfer, in which d is the distance between the RX and TX coils. If M is the mutual inductance of the two coils (inversely proportional to D), and $\omega = \frac{1}{\sqrt{L_{TX}C_{TX}}} = \frac{1}{\sqrt{L_{RX}C_{RX}}}$ is the resonant frequency, Infineon derives that the load appears to the TX as an impedance $Z = \frac{\omega^2 M^2}{R_{RX}+Z_L}$. Impedance matching is very important in achieving maximum power transfer, and as is clear from this formula, it requires an understanding of your load and your channel. [1]

Let $k = \frac{M}{\sqrt{L_{TX}L_{RX}}}$, then higher k yields a higher efficiency. Thus, a lower distance yields a higher efficiency, as do larger inductors. When the cochlear implant is surgically inserted, the RX is placed as close as possible to the outer ear. Physically, it lies just beneath the skin, and the TX is forced by a small magnet to be as close to the TX as possible. The channel between TX and RX is thereby only skin, which has a reported thickness in this region of 3 to 15 mm. Thus the distance cannot be made any smaller, and we can only vary inductances to make the system more efficient.

Aside from efficiency, however, the transmission frequency is also an important design parameter, which also constrains the inductance sizes. A review paper by Fan-Gang Zeng et al gives an overview of varying transmission properties between three commercially available cochlear implants: The Cochlear Nucleus Freedom, the Clarion HiRes 90k and the MED-EL MAESTRO. Their carrier frequencies and associated data rates are given in Table I. Notable is that a higher carrier frequency yields a higher data rate. [2]

Zeng et al elucidate a number of design tradeoffs associated with the design of the RF link. For example, a resonance circuit will be most efficient at its resonance frequency, which suggest a narrowband signal be sent. However, modulation schemes for digital transmission often require very large bandwidths. Another problem is coil size – larger coil sizes are more power efficient, but external coils are constrained by cosmetics, and internal coils are constrained by anatomy. For the cosmetic consideration, Figure 2 shows the external

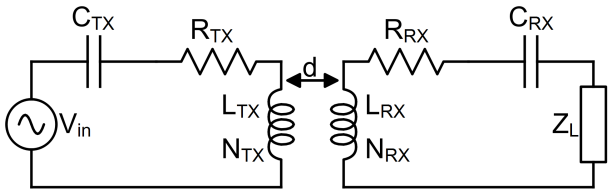

Fig. 1: The simple circuit at the heart of wireless power transfer.

Device	Carrier Frequency (MHz)	Data Rate (Mb/s)
Cochlear Nucleus	5.0	0.5
Clarion HiRes 90k	49	1.09
MED-EL MAESTRO	12	0.6

TABLE I: Carrier frequencies and data rates for three commercially available cochlear implant devices.

Fig. 2: The external component for a Nucleus Freedom, from Cochlear's online store.

Device	Battery Used	Battery Life
Cochlear Nucleus Freedom	3 Zinc-Air Batteries	3-5 Days
Clarion HiRes 90k	Lithium ion Battery	14-24 Hours
MED-EL MAESTRO	3 Zinc-Air Batteries	3-5 Days

TABLE II: Batteries for three commercially available cochlear implant devices.

component of the Cochlear Nucleus Freedom. It can be seen that it is designed to be flat, although not particularly small.

Further yet, considering that the size of an inductor is proportional to the resonance frequency, lower frequencies allow for smaller inductors but lower data rates. The RF link carrier frequency is thus a very difficult object to design around, and the power efficiency cannot be made close to 100% as a result. RF links, according to Zeng et al, achieve 40% power transmission efficiency, delivering between 20 and 40 mW of power.

The patent for the power transfer circuitry used in cochlear implants is held by Tae W. Hahn and Glen Griffith, and was filed in 2001. The patent presents a number of design challenges, including the fact that skin thickness is not constant, and the impedence of the RX load is not constant. This is because the electrodes sit in a fluid of varying characteristics. Their patent provides a schematic for a device which automatically matches the impedance between input and output, based on the reverse power signal from the RX back to the TX – this process is referred to as "back telemetry." This tends towards a situation in which optimal power transfer is possible. [3]

B. The Battery

Zeng et al compare the same three implants for battery life and battery type. Table II shows the batteries used and their expected lives. It is notable that the shortest battery life belongs not only to the device using a Lithium ion battery, but also to the device with the highest transmission frequency. Higher carrier frequencies and higher data rates require more power – this is one of the most fundamental trade-offs in electrical engineering.

Jing Fu et al in a review paper on Zinc-Air batteries provide some of the benefits of Zinc-air over Lithium ion batteries. While Lithium batteries have the highest specific energy, Zinc's energy density is comparable, and it is cheaper and more stable. The main draw to Zinc is one of volume – smaller Zinc batteries are more cheaply available, and small batteries are clearly preferable for the form factor of cochlear implants. [4]

Marcus Yip et al claim that for very low power applications, neither Lithium nor Zinc batteries are preferable. In fact, they claim that "ultra-capacitors" are preferable due to their small size. [5] They can also be cycled many more times than Lithium batteries. However, they are assuming a fully implantable circuit, wherein battery size is far more important. Their work is still important here, however, as any implantable low-power circuitry can also be implemented outside the body.

C. RX and TX Power Consumption

The battery on the TX side must power the DSP on the TX side, the RF transmitter and all circuitry on the RX side. On the RX side, Feng et al suggest that 20-40 mW are necessary to operate the RX side in most implants. This is assuming a 40% efficiency, implying that 50-100 mW are dissipated on the TX side. The TX side contains a DSP and a power amplifier, which themselves require power as well.

Yip et al have designed a low-power fully implantable implant. They claim that electrode stimulation itself requires 750 μw, and that all circuitry can be implemented such that it consumes only 250 μW. Zeng et al claim that in 2009, implantable ASICs designed for low power applications consumed only 129 μW. Thus, it is reasonable to assume a 1 mW power budget for the implanted circuit. It is fair to assume the TX-side circuitry consumes power on the same scale. Table III shows a reasonable power breakdown for a low-power cochlear implant.

Component	Power Consumed
DSP and Power Amplifier	130 μW
Implanted ASIC	130 μW
Electrode Stimulation	750 μW
Lost RF Power	1.32 mW
Total	2.33 mW

TABLE III: A low-power cochlear implant power budget assuming 40% efficiency in the RF link.

Notably, the RF loss is the most significant component – more than half of all consumed power. This suggests why low-power research has moved towards the fully implantable system in recent years, but as this technology is not yet in production, it is still valuable to consider its implications to conventional cochlear implants.

D. Photovoltaic Power Systems with Battery Storage

Utility-scale photovoltaic power systems with battery storage have been popular since the 1990s, and smaller-scale examples in digital electronics such as the calculator are popular as well. Chaurey and Deambi show in their 1991 review paper that the main challenge in photovoltaic power systems with battery storage is control around overcharging. [6] Permanent damage can be done to batteries via overcharging, so it must be avoided where possible.

While Chaurey and Deambi are focusing on the utility scale, the principles map down in scale. Any number of regulators presented in this paper could be applied to avoid both overcharging and rapid discharge. For example, the *automatic circuit breaking* method presented uses transistors to switch off current input to the battery when the battery is sufficiently charged.

A number of ICs exist which perform this regulation, but many of them depend on the chemistry of the used battery. A variation of the automatic circuit breaking topology using only components easily found in any laboratory is shown in Figure 3. An analysis of this circuit follows.

The driving force of the circuit is the linear voltage regulator – a 3-pin device which provides a constant voltage depending on the state of its adjust pin. The drop between the input and output voltage of the regulator is, at least, a volt or two so it is important that a solar panel with higher output voltage than the used battery is chosen. The diodes in the circuit similarly introduce a drop of about 1.4 V in total. The potentiometer is set depending on the desired battery voltage and the input voltage to provide a stable state for the regulator. The diodes are in place to make sure the battery does not discharge, and that current only flows out of the solar panel.

To analyze this circuit's operation, assume first that the battery has less charge than its maximum. In this case, diodes D_1 and D_2 will conduct and current will flow into the battery's positive terminal. Zener diode D_3 will not conduct so the transistor will act as an open switch and the adjust pin's value will be determined by the voltage divider formed by R_C and P. This is the "normal" operation.

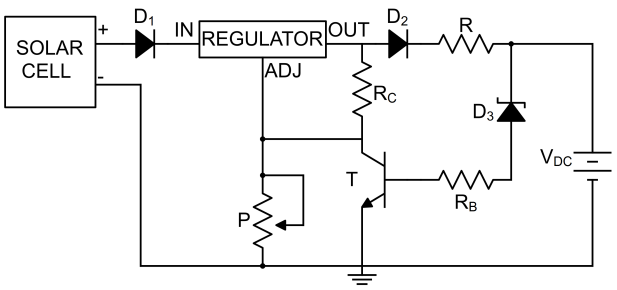

Fig. 3: A regulator schematic for charging the battery with the solar pannel.

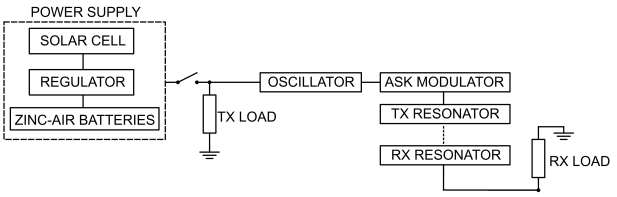

Fig. 4: A high-level block diagram for the system being designed.

Now suppose the battery overcharges significantly – the Zener diode will conduct in reverse, and the transistor will act as a closed switch, effectively shorting the adjust pin to ground. The battery will then stop charging, as the linear regulator will provide 0 V at its output.

While the overcharge protection circuitry is off, the battery absorbs power depending on the voltage at the output of D_2, and also is expected to generate power for the rest of the circuit. If the circuit is seen as a resistive load, which draws 2.33mW of power (as seen in Table III), the battery and solar cell must together produce this much power while the circuit is in use. When the circuit is not in use, the battery is only absorbing power rather than generating it. In this case, the battery absorbs power determined by the voltage at the output of D_2 and the resistance R.

III. Methods

A fully functioning cochlear implant will follow the block diagram shown in Figure 4. Within this diagram, the TX and RX loads would be a number of integrated circuits. In this simple proof-of-concept circuit, we are not going to implement the entire block diagram as shown, but simply a subset of it. For example, we will not include DSP hardware on either side of the circuit. Instead, we will implement only what is necessary to show the feasibility of a cochlear implant with a hybrid power source, according to the budget described in Table III.

The following section discusses the block diagram elements implemented, and theoretical expectations for each circuit.

A. The RF Link

1) Building the RF Link: The first blocks to be built are the wireless power transfer resonators. These blocks are, of course, critical for proper functioning of the device and must be in perfect working condition for the power characteristics of the system to be analyzed properly. Small-scale LC resonators are historically challenging to prototype due to the parasitic inductances and capacitance apparent in most prototyping boards. Solderless breadboards, while the easiest boards on which to build prototype circuitry, have remarkably high parasitic inductances across tracks. Alternatively, while printed circuit boards (PCBs) offer far lower parasitic inductances, they have unfortunately long lead times and don't allow for on-the-fly architecture changes.

To determine which of these testing methods is more viable we must first consider the oscillator frequency – for sufficiently high frequencies, resonance could never be achieved on a breadboard, and an alternative method would have to be chosen for prototyping. Table I shows that the lowest carrier frequency in production is 5 MHz, and driven by the ease of using breadboards, we choose to design the system around this frequency. Higher frequencies allow for higher bandwidths, but as the signal transmission aspect of cochlear implants is not being considered in this project, and as we know that 5 MHz is not destructively low, we do not lose out by picking such a low carrier frequency.

Give $\omega = \frac{1}{\sqrt{LC}}$, we can come up with ballpark estimates of inductor and capacitor values. Choosing small capacitor values allows for, relatively, larger inductor values, and as the parasitic inductance tends to be the larger problem on a breadboard, small inductor values are not feasible. Discrete 10 pF capacitors are commonly available, and choosing such a capacitor specifies an inductor value of about 100 μH.

Each breadboard manufacturer will create a product with different parasitics, so there is no clear way to estimate ahead of time what values will truly give resonance at 5 MHz, but with these ballpark values in mind, a series of values can be tested on a given breadboard with a function generator to find the components which truly give the desired behavior. Laboratory facilities at The Cooper Union were used to perform this test, as many discrete capacitors and inductors are readily available there.

2) Testing the Isolated RF Link: Once the desired LC values were obtained, a series of tests were performed using a function generator to simulate the oscillator and a probe to simulate a load. These tests constitute a critical validation step for this project – the RF link is where most power in the system is lost, as is clear from the power budget in Table III. The RF link should behave similarly when stimulated by a function generator as when it is stimulated by a local oscillator at a given frequency, so most power loss information can be extracted from these simple tests.

One performed test is for working distance – we want to see how well power is transferred at varying distances between RX and TX. We know theoretically that optimal performance will occur when the inductors are near, but in practice, they must be separated by a thin layer of skin. It is important to see how sensitive our system is to such small changes in distance. This is performed simply by measuring how ouput voltage changes across a given load for a fixed input signal as the inductors are moved further apart from one another.

We also test the bandwidth of the device. Both the TX and RX resonators have their own 3 dB bandwidth, and small component variations could cause these bandwidths to overlap less than entirely. That is to say that ideally the bandwidth of the RF link would be the bandwidth of either the TX or RX resonator, but in practice it will be smaller. We vary the input frequency without varying the input power to obtain the input frequencies at which the ouput power is 3 dB below the maximum.

B. The Oscillator and ASK Modulator

The oscillator, as described above, is initially modeled by a function generator when testing the RF link. The ASK modulator would exist in a proper cochlear implant, but as the bandwidth of the circuit is more easily measured in the isolated RF link with a function generator input, it is omitted in this early prototyping stage.

An IC square wave oscillator at 5MHz is used for later tests. A square wave oscillator is cheaper than a sinusoidal oscillator, which is why it is used, but it is important to realize that it is not power-efficient for our application. From a frequency content perspective, much of the power in a square wave lies outside of its fundamental, and those modes are not transmitted by the RF link. Thus, a large portion of the power in a square wave is wasted by the RF link.

As the power efficiency of the RF link is already known from the isolated RF link tests, and the power wasted in the higher harmonics of a square wave can be easily analytically determined, we still have all of the necessary tools with which to analyze the power consumed by the device.

C. The Power Supply

While Zinc-air batteries would likely be used in practice (as they are for most hearing aids), tests were performed mostly with Nickel metal hydride batteries. This was due to the incredible ease of access of rechargeable Nickel metal hydride batteries – local hardware stores sell rechargeable AAA batteries from Energizer, for example. The Zinc-air batteries used in hearing aids nominally have voltage of 1.45V, while rechargeable AA and AAA batteries have voltages of about 1.3V as well. The biggest drawback to AAA batteries in hearing aids is that they are large compared to coin batteries, but this problem is inconsequential in a test circuit.

As described in the literature review, the battery charger is implemented using an IC voltage regulator and a transistor to avoid overcharging (following Figure 3). Linear regulators can achieve almost any voltage below the voltage available at the input, but given the two diode drops between the solar cell and the battery, the cell must be at least at $2 \times (0.7V) + 1.3V$. We

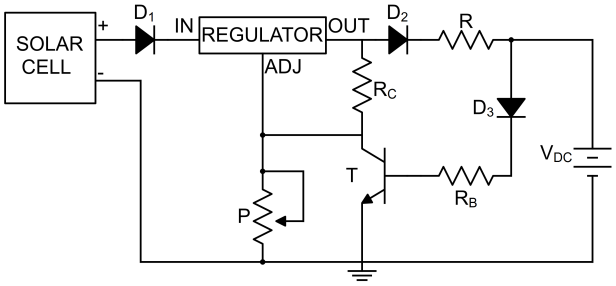

Fig. 5: An alternative regulator circuit for low voltages.

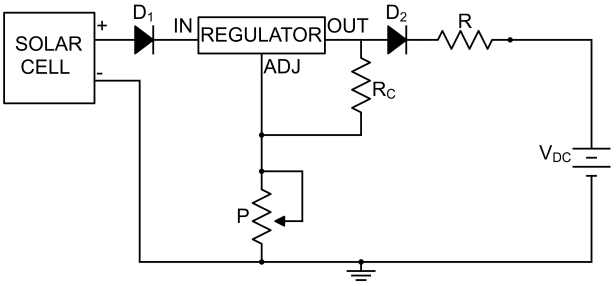

Fig. 6: A regulator circuit with no overcharging protection.

choose a 5V solar panel to have some room for voltage drops internal to the regulator, and variations in solar cell voltage.

Notable is the fact that a Zener diode is used in Figure 3. This is very nice for high voltage applications, but presents an unfortunate problem for our low output voltage circuit. We have two choices – we can either design a different mechanism for avoiding overcharging, or force the regulator to operate near the battery voltage. The latter will make it so that overcharging is never a problem, but it will also disallow our battery to charge quickly.

For the former, one could consider what would occur if the Zener diode in Figure 3 were replaced by a regular diode in the oppoite direction. This circuit, show in Figure 5, will turn off the regulator when the battery is charged to V_{BE} of the transistor plus one diode drop. This is a relatively low voltage in most cases, but for our application it is fine, as our battery should stay at only about 1.4 V – two diode drops.

However, a simpler circuit uses a lower bias on the regulator and removes the overcharge protection circuitry entirely. This circuit is shown in Figure 6. In this case, the regulator's output voltage will always be about the maximum battery voltage (plus a diode drop), so when the battery would begin to overcharge, the current across the resistor R would be 0. The clear loss here is that a higher output voltage allows for faster charging. We weigh these two options in testing.

The solar cell battery charger is tested alone before being applied to the circuit for safety purposes, using first a DC power supply to mimic both the battery and the solar cell. Once again, the laboratory spaces and resources at The Cooper Union were used to test this device, and the passives, regulator and transistor were provided by their laboratory staff.

D. The Switch

Linking the oscillator/RF link and the power supply is a switch. In cochlear implants, this switch is closed as a result of incoming sound. The implementation of such a trigger is outside of the scope of this project, and we will simply consider the cases where the switch is open and closed separately.

E. The Loads

While there is no clear value the loads on the RX or TX sides should take, the use of an oscilloscope probe as the RX load is natural for measurement purposes. Both loads in the block diagram are simplified representations of the power drawn by ICs which are not used in our power experiments. They need not actually play the role of consuming power in our experiments, as we can simply refer to the power budget provided in Table III to determine the magnitudes of losses apparent in a real system. Thus, the TX load need not be implemented but rather only theoretically considered.

IV. Equipment and Components

The majority of experimental data has been recorded using an oscilloscope provided by The Cooper Union, with probe resistance of 1 MΩ and capacitance of 11 pF. For RF link experiments, the function generator used is a BK Precision 4040A provided also by The Cooper Union. The solderless breadboard, all used passives, transistors, diodes and regulators were provided by The Cooper Union as well. Energizer brand rechargeable AAA batteries and AMX3d 5V 30mA micro mini solar panels were used. The regulator IC used is an LM317, the dididoes used are 1N4148 signal diodes and the transistor used is the PN2222. The oscillator used is a EXS-100A 5.0000 MHz oscillator.

V. Results

A. The RF Link

1) Finding 5MHz Resonance: In determining the RF link component values that gave 5MHz resonance on a solderless breadboard, it was important to consider the effect of the oscilloscope probe's capacitance on the resonant frequency. The used oscilloscope has a capacitance of 11 pF, which was almost exactly the designed capacitance of 10 pF. With this in mind, we simply changed the inductor value, with one half of the circuit using a discrete capacitor and the other using the probe capacitance to achieve resonance. This is as shown in Figure 7.

Using 100 μH inductors, as designed, gave far too high a resonant frequency. This is due, likely to parasitic capacitors and inductors in the solderless breadboard. Considering the resonance equation, an additional series inductance in the conduction path will increase the resonant frequency from the ideal, thus the inductor value was lowered until 5MHz resonance was found. 33μH inductors gave resonance at about 4.75MHz, implying a relatively high parasitic inductance as

expected. While this is not exactly 5 MHz, it is the closes to 5 MHz we were able to achieve with the available discrete components. The physical test circuit can be seen in Figure 8.

2) Distance Dependence: We know that a distance of only 3 to 15 mm is seen in practice between the two inductors, as stated in the literature review. In this experiment, we use oscilloscope probes on both sides of the RF link rather than capacitors, and measure the input and output voltages at 3 inductor distances – 1 inch apart, half an inch apart and one quarter of an inch apart. In mm, this is about 25 mm, 13 mm and 6mm respectively. It was very hard to achieve stable distances nearer than 6mm apart without the inductors simply touching.

Unsurprisingly, we see that the voltage across the output shrinks significantly as the inductors are moved further apart. Table IV summarizes the results found. It is clear that at one quarter inch, the efficiency is quite good – even better than the expected 40%. However, at the larger values of distance, the efficiency is not acceptable. Given most skin varies in thickness between less than one quarter of an inch and slightly more than one half of an inch, it is believable that this link could achieve 40% efficiency in a human subject.

Figures 9a, 9b and 9c show TX and RX voltage waveforms on the oscilloscope with one quarter inch, one half inch and one inch separation respectively..

3) Bandwidth: To find the 3 dB bandwidth of the RF link, we consider the RF link at some fixed distance such that the TX peak-to-peak voltage is 0.5 V at 5 MHz. The 3 dB frequencies occur for the TX portion when the input reaches 500mV/$\sqrt{2}$, which is approximately 350 mV. Figure 10a shows the RX and TX voltages at this instance. We sweep the input frequency up until this occurs, at approximately 5.2 MHz, and down until this occurs at approximately 4.2 MHz. Figures 10b and 10c show the voltage waveforms at these frequencies. We knew that the resonant frequency of the circuit is closer to 4.75 MHz, and these values are relatively symmetric about that resonant center frequency. Thus, the TX portion has about 1MHz 3 dBb bandwidth centered about 4.75 MHz.

We look also at the RX portion (as seen in the Figures 10a, 10b and 10c) and see that it drop significantly lower at these frequencies than the TX portion of the link. More specifically, what we find to be the 3 dB bandwidth for the TX portion is actually the 6 dB bandwidth for the RX portion. This is due to mismatches in component values on either side of the link due to parasitics as well as component manufacturing errors.

The data rate given for the Cochlear Nucleus in Table I is 0.5 MB/s. By Nyquist's theorem, such a data rate will require a bandwidth of at least 1 MHz. If 6 dB bandwidth is acceptable, then we have achieved a Nyquist-viable system. If 3 dB bandwidth is acceptable, while 6 dB bandwidth is not, a more precisely built system is required. As we used a solderless breadboard rather than a PCB, this is actually quite fortunate – to achieve near-acceptable values with such a deeply imprecise prototype speaks to the robustness of this simple design.

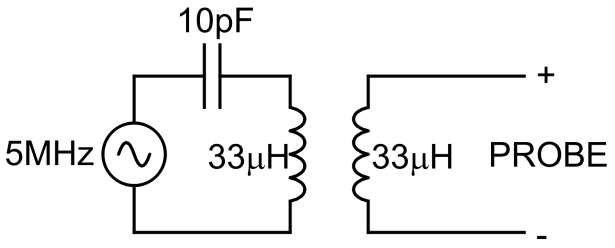

Fig. 7: Schematic of the RF Link circuit used for measurements, wherein the probe on the right-hand side serves both as a measurement instrument and as an 11 pF capacitor. If both sides were to be measured at once, both capacitors would be replaced by oscilloscope probes.

Distance	Pk-Pk V_{out}/V_{in}	Power Efficiency
0.25 in	0.75	56.25%
0.5 in	0.13	1.7%
1 in	0.01	0.02%

TABLE IV: A table showing the distance dependency of the RF link efficiency.

Whether or not 3 dB or 6 dB bandwidth is acceptable is, of course, dependent upon one's SNR. However, we must remember that cochlear implants are not only sending signal but power as well. While the system is likely to have high SNR (the channel is skin, and no other RF signals in the 5 MHz range are present), a 6 dB loss in transmitted power could have catastrophic consequences on the RX power.

It is worth noting that the bandwidth of an LC circuit is related to the series resistance of the circuit – a larger series resistance results in a larger bandwidth, but also implies a lower amplitude at the resonant frequency. Here our series resistance is entirely incidental (partly due to contact resistances on the breadboard) and not a parameter that we have designed around. However, if we wanted to achieve a higher bandwidth, we could add series resistance, with the understanding that it would absorb power and thus further decrease our power efficiency. This power bandwidth tradeoff is a fundamental principle of electrical engineering, and even in this incredibly simple case it is inescapable!

B. The Power Supply

The regulator circuits as shown in Figure 5 and 6 are built with discrete components isolated from the rest of the circuit. At first, they are built with simulated sources instead of solar cells or batteries, so as to ensure that the circuit works before potentially damaging equipment. These circuits worked exactly as expected, with the alternate overcharge protection circuit activating at about 1.4 V with the transistor used. To achieve these results, we use a 50kΩ potentiometer, let $R_C = 220\Omega$, $R_B = 330\Omega$ and $R = 220\Omega$.

Next, we hook up the solar cell and battery. The solar cell is rated at 5V, but its voltage varies slightly depending on the

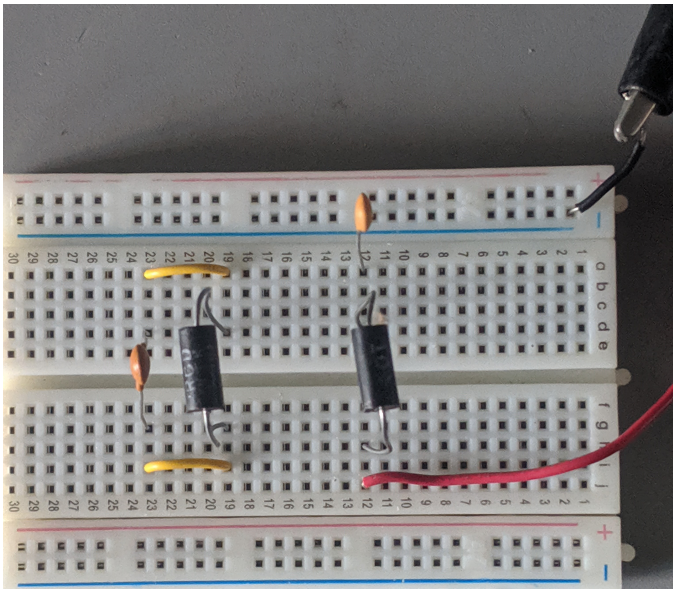

Fig. 8: Prototype RF link setup on solderless breadboard, without oscilloscope. Right-hand side is TX, where the red wire is the function generator input. The black discrete components are 33 μH inductors, and the orange circular components are 10 pF capacitors.

directness of sunlight. In complete darkness, its voltage is not high enough to provide a voltage above the battery voltage at the output side of diode D_2. This is expected, and due to the diodes in the circuit, the battery will simply discharge while the solar cell remains ineffective in cases such as this one. In indirect and direct lighting conditions, the voltage is high enough to charge the battery.

With the component values used, we see about 1V is dropped across the regulator, and 1.4V are dropped across the diode. Thus, about 2.6V are available at the output of D_2 in direct sunlight. With a 220Ω resistor, and a 1.3V battery, about 7mW of power are absorbed by the resistor in direct sunlight conditions. This also provides about 6mA of current – with the 1.3 V battery voltage, this is more than enough to power the entire circuit and also charge the battery, as the circuit should only require 2.3 mW of power according to III. That is to say that this circuit, in direct sunlight, can be powered entirely by the solar cell and also continue to charge for later use.

In indirect sunlight, the results can vary wildly. Of course, the other extreme case is that the solar panel generates no power at all in complete darkness. However, given that the main use case of a cochlear implant is in a lit room, most implants will receive at least enough light to generate some power and at least increase the battery life of the device.

The solar cell used was chosen to be small and inexpensive. Figure 13 shows the solar cell with a nickel for scale – it should be noted that this is not quite small enough to be implemented comfortably above the ear.

C. The Entire Circuit

Putting the RF link, power supply and oscillator together, we get our full prototype circuit. Considering the power efficiency of a square wave oscillator with a 50% duty cycle, it is made clear that half of the input power to the system is lost in the oscillator. As our solar cell should supply more than twice the needed power for operation to the circuit in direct sunlight, we expect to still see acceptable values. Measuring again at the RX side with an oscilloscope, we see the output voltage in direct sunlight at one quarter inch inductor separation as shown in Figure 11.

We see that the output is a sine wave, with 0.82V peak-to-peak. This, compared to an input at 1.3V peak-to-peak, gives approximately a 40 % efficient RF link as desired.

The state of the breadboard in this final implementation can be seen in Figure 12.

VI. Theoretical Implementation

This solderless breadboard implementation is a step towards a more practical implementation of a cochlear implant, but it is worth considering whether or not a cochlear implant with this architecture could ever be implemented within reasonable constraints. First, we should realise that we have not added any components to the RX side, and thus we should focus on the size of the TX.

To determine more realistic size constraints, a printed circuit board (PCB) was designed for the TX circuitry using KiCad. The schematic on which this PCB is based is exactly the implemented circuit, but with a coin battery holder in place of the battery, and discluding the solar cell which would necessarily lie out of plane with the rest of the circuit. Component sizes are determined using readily available surface-mount ICs and passives, as well as some through-hole components. As shown in KiCad's 3D viewer, the PCB is shown in Figure 14. This PCB came out to be 22mm $\times$ 31mm, far smaller than the current cochlear implant implementations. This is despite not being too aggressive with component sizes.

It should be noted that a number of components are missing from this design. Namely, the microphone, DSP and ASK modulator are not shown here. In standard cochlear implants, the microphone usually rests in the ear of the user, away from the rest of the circuitry.The DSP and ASK modulator would likely be implemented on a small microprocessor IC, which will add a bit of surface area to the device. However, even if one dimension were doubled by such an addition, this device would still be reasonably wearable.

The other missing item is, of course, the solar cell. The cell should be thin, and should coat the device. Solar cells in the 5V range at this size are available, such as the Voltaic Systems "Small" series of solar panels. Cochlear implant manufacturers with more resources could even manufacture custom cells for this purpose, perhaps even of the thin film variety.

It should be noted that the solar cell need not actually be worn above the ear. For people with long hair, for example, this is a particularly non-ideal position. It is possible that the cell could be worn on clothing so that more energy could

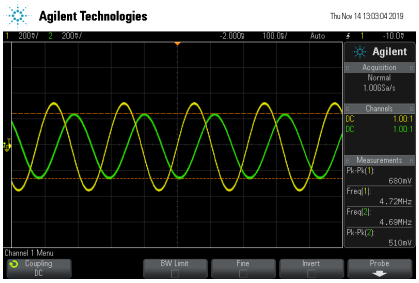

(a) TX (channel 1) and RX (channel 2) voltage waveforms at one quarter inch separation.

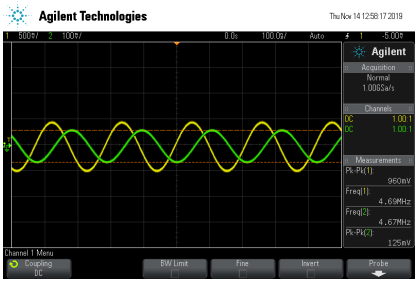

(b) TX (channel 1) and RX (channel 2) voltage waveforms at one half inch separation. Note the division size in voltage.

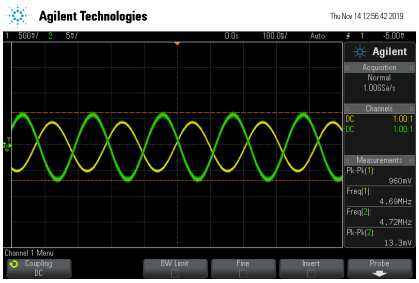

(c) TX (channel 1) and RX (channel 2) voltage waveforms at one inch separation. Note the division size in voltage.

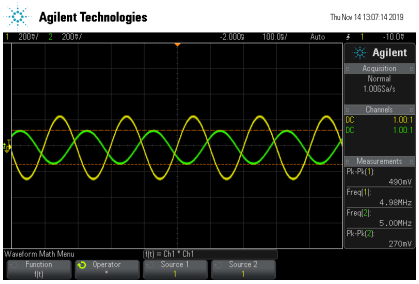

(a) TX (channel 1) and RX (channel 2) voltage waveforms at 5MHz.

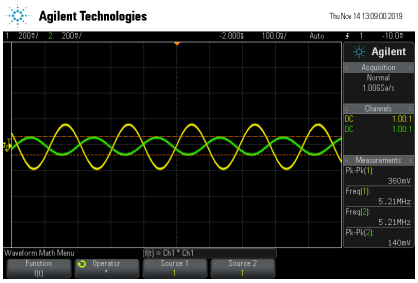

(b) TX (channel 1) and RX (channel 2) voltage waveforms at the TX upper cutoff frequency.

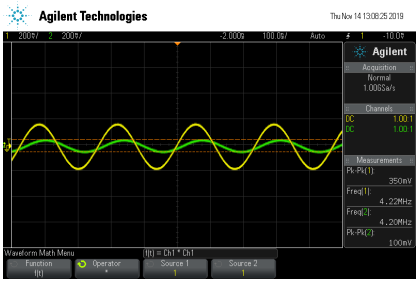

(c) TX (channel 1) and RX (channel 2) voltage waveforms at the TX lower cutoff frequency.

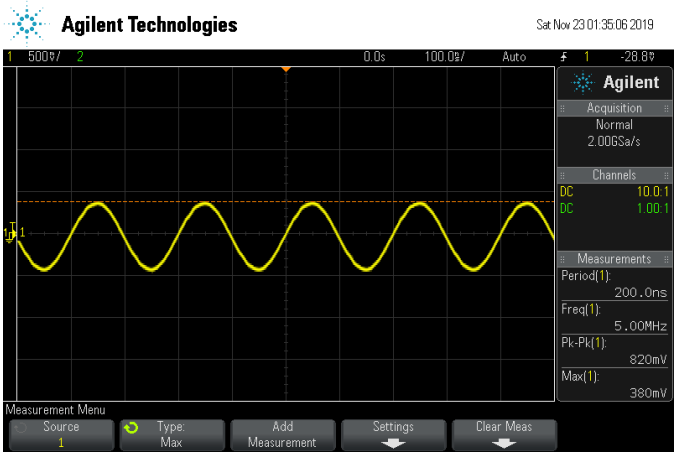

Fig. 11: Output on the RX side of the RF link at about quarter inch separation with the entire circuit in use, in direct sunlight.

be gathered from sunlight, but this introduces a problem in fashion that ought not be solved by electrical engineers!

VII. Conclusions

We have shown that, leveraging recent developments in low power implant circuitry, the use of a hybrid solar power source can greatly increase battery life for cochlear implants. Better yet, we have shown that in direct sunlight, such an implant could maintain battery life for an arbitrarily long period of time. This being achieved despite the fact that a square wave oscillator was used rather than a sine wave oscillator and a

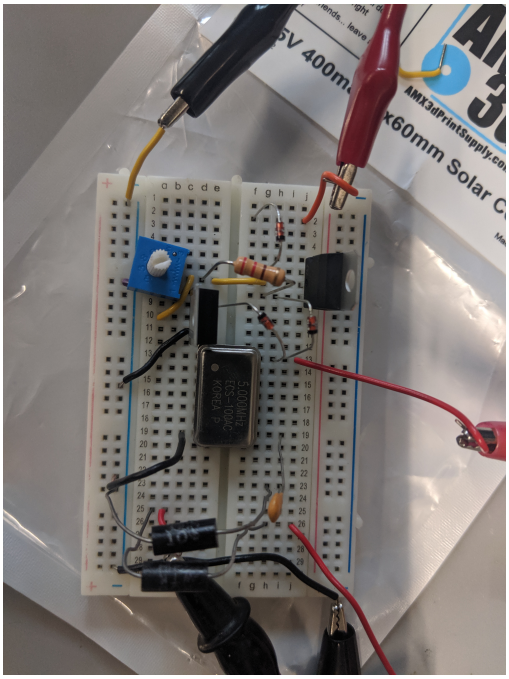

Fig. 12: The prototype circuit on the solderless breadboard.

solderless breadboard was used rather than a printed circuit board speaks to the feasibility of this design.

The size of the implemented device is, in this prototype stage, too large. However, the components used are invariably available at far smaller sizes, and the rough PCB sketch shows

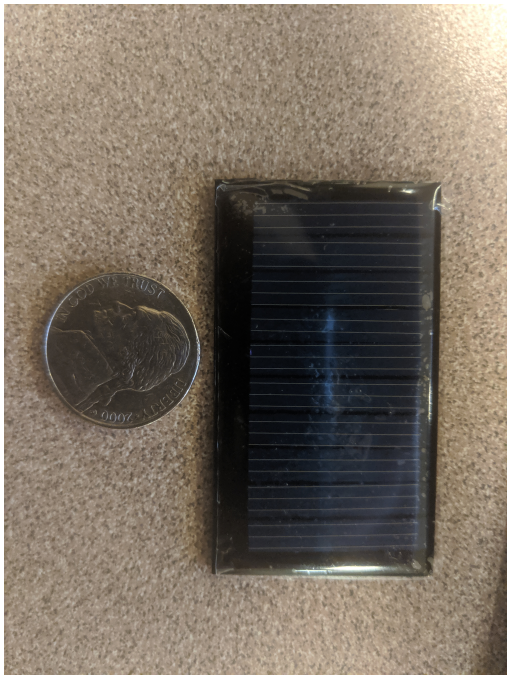

Fig. 13: Solar cell used with nickel for scale.

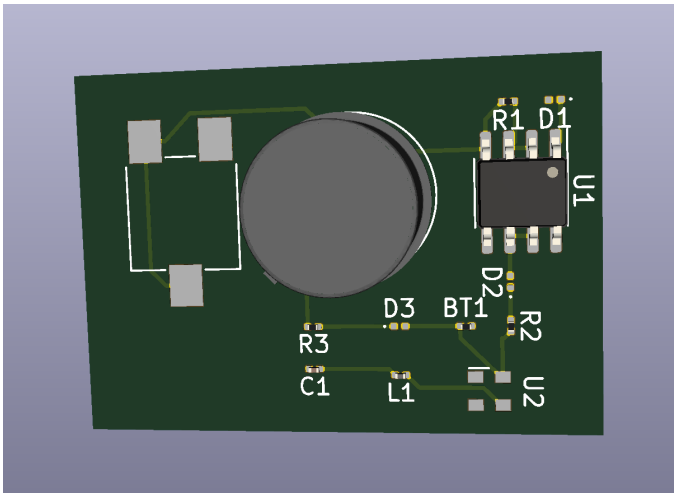

Fig. 14: TX circuitry on a PCB, shown in KiCad's 3D viewer.

that a reasonably sized hybrid cochlear implant is feasible.

While there is reason to believe such an implant could be made, it is unfortunately the case that higher-power cochlear implants still dominate the market. This is due to the fact that low-power developments have been specified to the fully implantable cochlear implant field, and also due to these developments being relatively recent. The proposed design serve as a middle ground – while fully implantable devices are not yet on the market, lower power devices with hybrid power sources are completely viable, as this prototype shows.

The choice of solar power for this project is rightly vulnerable to criticism – a device worn on the side of one's head will not necessarily receive direct sunlight. While many hairstyles would allow for a device mounted above the ear to receive light from above, many would find the device's light source obfuscated by hair. While solar power was explored here due to its ease of access, there are other hybrid power sources that could be considered just as well. For example, one could consider using the temperature gradient along one's skin as a source of power which is independent of hairstyle.

References

[1] S. Schaecher, "Resonant wireless power transfer," white Paper 05-2018.

[2] F.-G. Zeng, S. Rebscher, W. V. Harrison, X. Sun, and H. Feng, "Cochlear implants:system design, integration and evaluation," *IEEE Reviews in Biomedical Engineering*, vol. 1, 2009.

[3] T. W. Hahn and G. A. Griffith, "Power transfer circuit for implanted devices," U.S. Patent 6 212 431 B1, Apr. 3, 2001.

[4] J. Fu, Z. P. Cano, M. G. Park, A. Yu, M. Fowler, and Z. Chen, "Electrically rechargeable zinc–air batteries: Progress, challenges, and perspectives," *Advanced Materials*, vol. 29, 2016.

[5] M. Yip, R. Jin, H. H. Nakajima, K. M. Stankovic, and A. P. Chandrakasan, "A fully-implantable cochlear implant soc with piezoelectric middle-ear sensor and arbitrary waveform neural stimulation," *IEEE Journal of Solid-State Circuits*, vol. 50, 2015.

[6] A. Chaurey and S. Deambi, "Battery storage for pv power systems: An overview," *Renewable Energy*, vol. 2, 1991.